03,07

Detection and study of 60°-rotation domains in α-Ga_2O_3 using transmission electron microscopy

© A.V. Myasoedov[1], I.S. Pavlov[2], A.I. Pechnikov[1,3], V.I. Nikolaev[1,3]

[1] Ioffe Institute,
St. Petersburg, Russia
[2] Shubnikov Institute of Crystallography „Crystallography and Photonics", Russian Academy of Sciences,
Moscow, Russia
[3] Perfect Crystals LLC,
St. Petersburg, Russia

E-mail: amyasoedov88@gmail.com

Received August 23, 2022
Revised August 23, 2022
Accepted September 6, 2022

The conditions have been established for detection and recognition of rotation domains in α-Ga_2O_3/α-Al_2O_3 (0001) thin films in the presence of other polymorphs. The domains are visualized by high-resolution transmission electron microscopy. Their structural characteristics are determined by preparing cross-sectional and plan-view specimens, choosing the correct diffraction conditions and proper imaging modes. As a result, the dimensions, the spatial distribution, the volume fraction and area fraction of the inclusions of domains have been determined.

Keywords: structural defects, rotational domains, transmission electron microscopy, gallium oxide.

DOI: 10.21883/PSS.2023.01.54972.463

1. Introduction

Gallium oxide (Ga_2O_3) is a semiconductor material that crystallizes in the form of various phases that differ from each other in the band gap and other physical properties. Epitaxial films of four known polymorphic modifications Ga_2O_3 can be synthesized in the laboratory by varying growth parameters such as temperature and pressure. The band gap width between different modifications varies from 4.5 to 5.3 eV (see, for example, overview [1]). Obtaining single crystals of high structural perfection by crystallization from a melt under normal conditions is possible only for the thermodynamically stable β-phase (4.48 eV [2]), which is already used for the manufacture of electronic devices [3]. Other polymorphs Ga_2O_3 are metastable, and there are very few reports in the literature about obtaining single crystals of these phases [4]. At the same time, they are grown by low-temperature vapor phase epitaxy in the form of thin layers.

All known polymorphs Ga_2O_3 are of steady and deep interest to researchers because of their unique properties. In particular, the α-phase has the largest value of the band gap width: 5.0−5.3 eV [5]. Monocrystalline films of this phase are obtained by heteroepitaxy, for example, by the method of chloride vapor phase epitaxy on sapphire substrates [6]. The films are used for experiments on the development of devices with exceptional parameters [7], which have a relatively low cost.

Crystals α-Ga_2O_3 have a corundum structure, the elementary cell of which belongs to the space group $R\bar{3}c$ of a trigonal crystal system described by rhombohedral or hexagonal coordinate systems. In α-Ga_2O_3, oxygen ions form a structure of alternating weakly distorted densely packed layers, while gallium ions occupy two-thirds of the octahedral voids between them [8]. Alternation occurs along the directions [0001] or [111], respectively, in hexagonal or rhombohedral systems. In the literature devoted to the study of α-Ga_2O_3, the crystal lattice is described in a hexagonal coordinate system with parameters $a_0 = 4.98$ Å and $c_0 = 13.43$ Å, therefore, in the work to denote the crystallographic indices of planes and directions, we will adhere to the Bravais–Miller system. Layers of α-Ga_2O_3 with a high degree of crystallinity [9] are obtained on the sapphire substrates with orientation (0001). However, the layers contain structural defects, in particular, threading dislocation distributed with a density of order 10^{10} cm^{-2} [5]. Technological efforts to epitaxial growth of the phases γ- and κ-Ga_2O_3 on sapphire in the best cases lead to the formation of rotation domains [10] in the films. In the worst cases, the films include aggregates of small crystals of various orientations.

A steadily recurring feature of the domain structure is the rotation of domains around the direction of alternation of densely packed gallium and oxygen layers, which are usually slightly distorted. Particularly, in the films β-Ga_2O_3, six types of differently oriented domains are formed around the normal to the plane $(\bar{2}01)$ [11,12]. Three variants of domains rotated relative to the direction ⟨001⟩ [10,13,14] were found in the films κ-Ga_2O_3. Finally, two variants of domains rotated around the direction ⟨111⟩ [15,16] were revealed in the films γ-Ga_2O_3. These features can be explained by

the lower symmetry of the lattices of the listed polymorphic modifications with respect to the rotations and reflections inherent in the corundum lattice, that is, the absence of a threefold axis of symmetry.

In contrast to the low-symmetry phases, α-Ga_2O_3 polymorph on sapphire substrates is obtained as structurally homogeneous monocrystalline films. Nevertheless, the literature data [17] and our own results allow us to conclude that domains rotated relative to the matrix by 60° around the c axis can form in films. An additional set of peaks in X-ray diffraction corresponding to such domains was observed for samples whose azimuthal position changed by 60°. The weak intensity of the reflections indicated that the domains were present as inclusions. In the article [17], the intensity of additional peaks was estimated and it was shown that the volume fraction of inclusions was 0.4%. Such domains can be characterized as rotation twins, however, to preserve the terminology adopted in the literature on Ga_2O_3, we will use the term rotary domain. Despite the relevance of the task of obtaining films α-Ga_2O_3 that do not contain rotation domains [17], the structure of such defects and the conditions for their formation remain poorly understood.

This paper presents the results of an analysis of the conditions for detecting and investigating the properties of inclusions of 60°-rotation domains in films of α-Ga_2O_3, performed by transmission electron microscopy (TEM). The films were synthesized on the basal-plane sapphire. The spatial arrangement of domains is clearly shown and their characteristics are determined: size and volume fraction. Recommendations for the diagnosis of rotation domain inclusions by the TEM techniques are described here.

2. Experimental procedure

Thin α-Ga_2O_3 films were grown by halide vapor phase epitaxy (HVPE) on (0001) sapphire substrates. The synthesis was carried out at atmospheric pressure in a horizontal quartz reactor developed in Perfect Crystals LLC [6]. The growth rate varied from 8 to 12 $\mu m \cdot h^{-1}$, and the formation of films of a given thickness was determined by the duration of the growth process. Four samples with layers of thickness from 0.8 to 1.3 μm were selected for the study by the TEM. The films had a mirror-smooth surface. In the above thickness range, no significant differences in structural properties were detected, and the presence of inclusions of 60° rotation domains was confirmed for all four samples.

The experiments were carried out in an Osiris (Thermo Fisher Scientific, USA) scanning/transmission electron microscope (S/TEM) at an accelerating voltage of 200 kV. Specimen preparation in different orientation for transmission and scanning transmission electron microscopy (TEM/STEM correspondingly) analysis were carried out on a dual-beam scanning electron microscope (SEM) Scios (ThermoFisher Scientific, US) equipped with a focused ion beam (FIB) system. For our study we choosed orientations in cross-section and parallel to the basal plane of epitaxial structures. For the orientation of the sample during the observations, a double-tilt holder with an inclination of ±35 and ±27 degrees along two axes was used.

To identify the rotation domains in the images obtained by TEM, it is necessary to understand diffraction selection rules for allowed reflections of this structure. Let us look at these rules in more detail.

Below the reflection conditions for the space group $R\bar{3}c$ are represented [18]:

$$\begin{aligned} hkil: &\quad -h+k+l=3n,\\ hh\overline{2h}l: &\quad l=3n,\\ h\bar{h}0l: &\quad h+l=3n,\ l=2n,\\ 000l: &\quad l=6n. \end{aligned} \tag{1}$$

The indices for planes of inclusions rotated by 60° around the c axis relative to the matrix can be found in a coordinate system rigidly connected to the matrix using the following rotation transformation:

$$\begin{pmatrix} h^* \\ k^* \\ l^* \end{pmatrix} = \begin{pmatrix} -1 & 0 & 0 \\ 0 & -1 & 0 \\ 0 & 0 & 1 \end{pmatrix} \begin{pmatrix} h \\ k \\ l \end{pmatrix}, \tag{2}$$

where h^*, k^*, l^* are the indices of the inclusion planes written in the coordinate system of the matrix. Here we also took advantage of the fact that a turn by 60° for this structure is equivalent to a turn by 180°, since the axis $\bar{3}$ can be considered as an independently acting axis 3-th of the order and the center of symmetry. The diffraction selection rules for allowed reflections should also be transformed taking into account (2). We are interested in two conditions: $-h+k+l=3n$ and $h+l=3n$, where $l=2n$. Using the relation (2), we obtain similar conditions for inclusions: $h^*-k^*+l^*=3n$ and $-h^*+l^*=3n$, where $l^*=2n$. If the area observed in the TEM contains an overlay of the matrix and inclusions, then both types of reflexes will be observed on the electronogram from this area. Below we give some examples of the description of such reflections

$$\begin{aligned} -h+k+l=3n &\qquad 01\bar{1}\bar{2},\ 01\bar{1}4;\\ h^*-k^*+l^*=3n &\qquad 01\overline{\bar{1}2}^*,\ 01\overline{\bar{1}4}^*;\\ h+l=3n,\ l=2n &\qquad 2\bar{2}0\bar{2};\\ -h^*+l^*=3n,\ l^*=2n &\qquad \bar{2}20\overline{\bar{2}}^*. \end{aligned} \tag{3}$$

3. Results and discussion

Figure 1, *a* shows a high-resolution TEM (HRTEM) of the superposition of the crystal lattices of the matrix and inclusion when oriented along the $[\overline{2}110]$ zone axis. For clarity, the overlay area is highlighted with dotted lines in

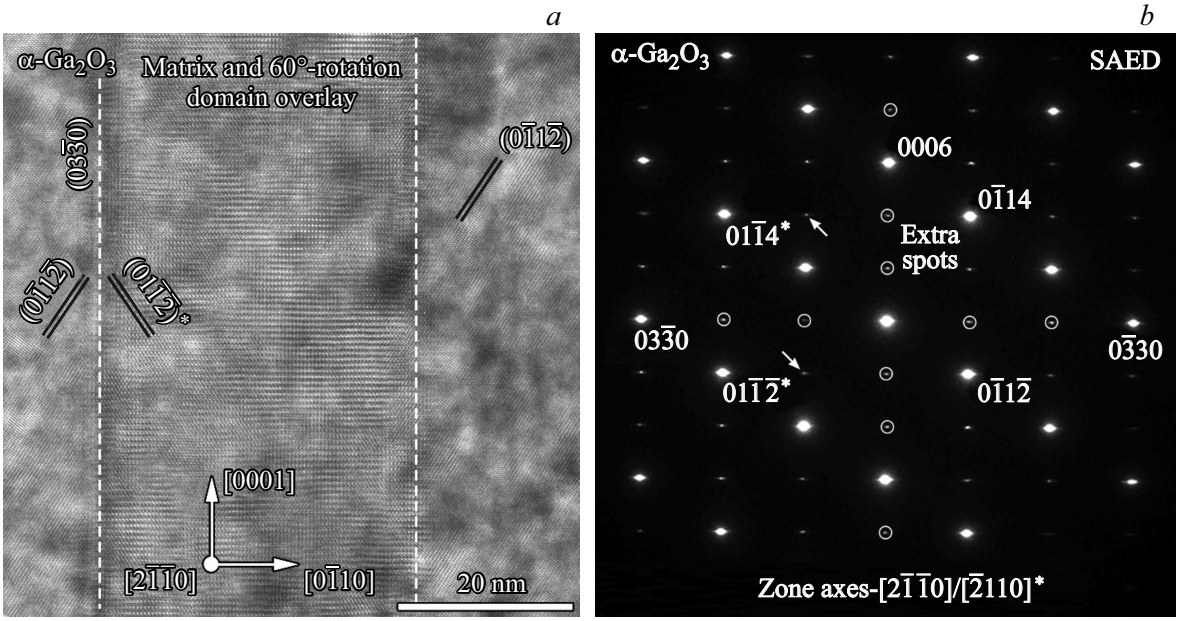

Figure 1. *a* — HRTEM image and *b* — SAED pattern corresponding to the area of overlay of matrix and inclusion of 60°-rotation domain when the cross-section is oriented along the zone axis $[2\bar{1}\bar{1}0]$. Forbidden reflections resulting from double diffraction of electron rays are circled.

the image. The oblique lines mark the position of the atomic planes $(0\bar{1}\bar{1}2)$ corresponding to the largest interplane distance for the considered zone axis. Fig. 1, *b* shows the selected area electron diffraction (SAED) pattern, that was received from this region. Reflections caused by the inclusion of 60°-rotation domain are indicated by asterisks and indicated taking into account additional conditions (3). The reflections generated due to double diffraction are marked with circles.

It can be seen from SAED that additional reflections are characterized by a weaker intensity than reflections from the matrix. Please note that when indexing atomic planes by Fourier analysis of the HRTEM image (Fig. 1, *a*), the values of the reflection intensities of the matrix and inclusion will be lost for the Fourier spectrum. A large number of polymorphic modifications with close interplanar distances can lead to an incorrect interpretation of the observed pattern.

We also note that when observing along the zone axis $[1\bar{1}00]$ the planes of the matrix and inclusions duplicate each other. Therefore, it is impossible to identify rotation domains in this orientation. Therefore, the zone axis like $\langle 1\bar{1}00\rangle$ cannot be used to identify inclusions of this kind.

Analysis of the results of the study of cross-sections of samples allows us to conclude that inclusions occur at the interface with the substrate. They propagate longitudinally from the interface to the surface of the film. Their size in the transverse direction can be several tens of nanometers. Inclusions, as a rule, have flat vertical boundaries with the matrix.

Cross sections of the samples in planar geometry (0001) were prepared in order to determine the shape and transverse dimensions of the rotation domains and estimate their distribution. To observe inclusions against the background of the matrix, it turned out to be very convenient to use bright-field STEM in combination with a strong slope of the sample.

For the zone axis $[000\bar{1}]$, the atomic planes of the matrix and inclusions duplicate each other, which is similar to the case with the zone axis $[1\bar{1}00]$. Because of this inclusion does not appear against the background of the matrix on HRTEM- and STEM-images of the sample (Fig. 2, *a*). To detect inclusions, the sample should be oriented so that the electrons diffract differently on the matrix and inclusions. For this purpose, the sample should be tilted relative to the position to be observed in the axis of the zone [0001]. This technique revealed a significant number of inclusions in the film (Fig. 2, *b*).

Undesirable inclusions of other polymorphic modifications are often found in the layers of metastable phases of gallium oxide. In order to confirm the correspondence of the observed inclusions to the 60°-rotation domains of the α-phase, HRTEM images were additionally obtained. On them, inclusions against the background of the matrix are represented in the zone axes, for which the atomic planes do notcompletely duplicate each other. Using the Kikuchi lines, we can rotate the sample in the double-tilt holder around an axis parallel to the direction $[\bar{1}120]$ of the sample. This makes it much easier to obtain the desired orientation of the sample. The zone axes used to identify inclusions were selected taking into account the

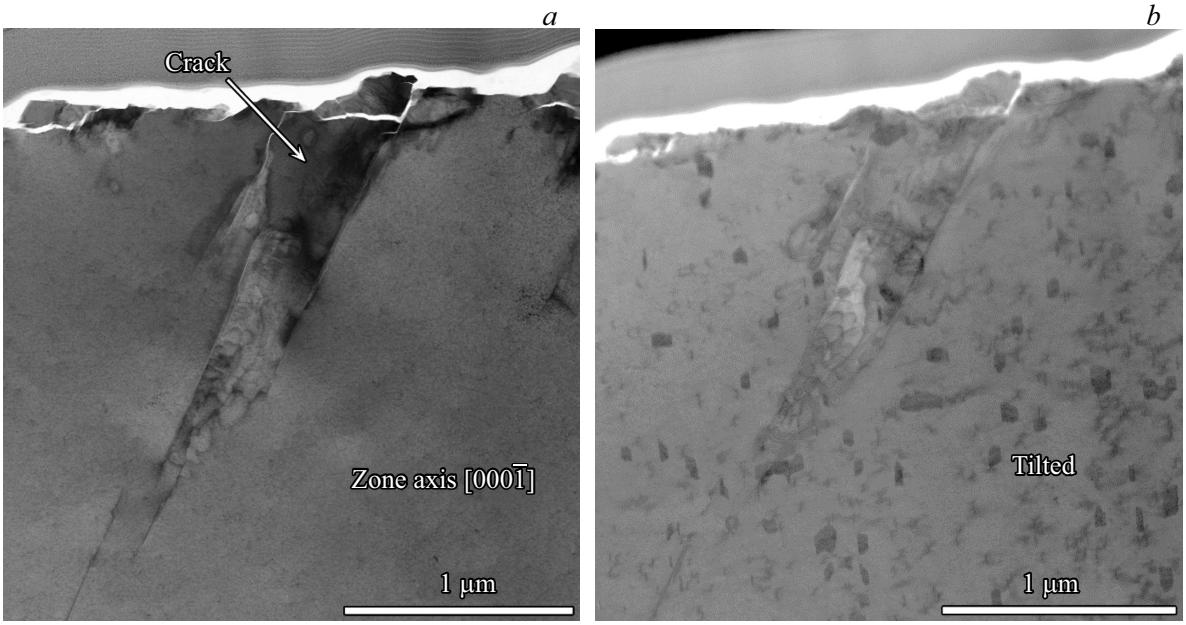

Figure 2. The bright-field STEM-images of the same cross-sectional area of a sample prepared in planar geometry. *a* — direction [000$\bar{1}$] of the sample α-Ga_2O_3 parallel to the electron beam, *b* — the image was taken with a strong inclination of this direction with respect to the electron beam. The arrow marks a crack that occurred during sample preparation.

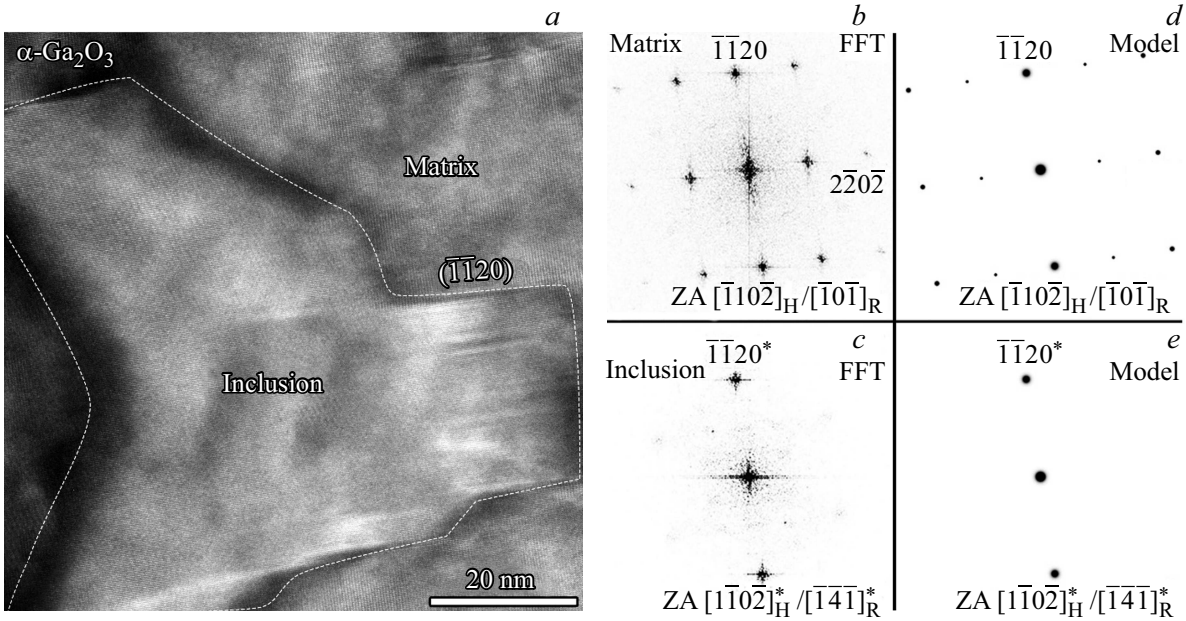

Figure 3. *a* — HRTEM image of the inclusion of 60°-rotation domain, against the background of the matrix. The directions [1$\bar{1}$0$\bar{2}$] and [$\bar{1}$10$\bar{2}$]*, respectively, of the domain and the matrix are oriented parallel to the electron beam. *b, c* — two-dimensional Fourier transforms corresponding to the regions of the matrix and inclusion in the HRTEM image. *d, e* — simulated images of the diffraction pattern for zone axes, respectively [$\bar{1}$10$\bar{2}$] and [1$\bar{1}$0$\bar{2}$]* α-Ga_2O_3.

allowed reflections [see system of equations (3)]. They are listed in the table, where next to the directions recorded in the hexagonal coordinate system, their notation in the rhombohedral system is given. This is done in order to emphasize the differences between the zone axes for the inclusion and the matrix.

The HRTEM image of one of the inclusions is shown in Fig. 3, *a*. In this case, the matrix and the inclusion are oriented respectively along the axes of the zone [$\bar{1}$10$\bar{2}$] and [1$\bar{1}$0$\bar{2}$]*. Figure 3 shows two-dimensional Fourier transforms of inclusion lattices (*b*) and matrices (*c*). The second one contains only peaks corresponding to the

Values of the angle φ between the crystallographic directions of the matrix and inclusions with the zone axis $[000\bar{1}]$ when rotating around the $[\bar{1}\bar{1}20]$ direction

Matrix	Inclusion	φ, °
$[000\bar{1}]_H/[\bar{1}\bar{1}\bar{1}]_R$	$[000\bar{1}]^*_H/[\bar{1}\bar{1}\bar{1}]^*_R$	0
$[\bar{1}10\bar{5}]_H/[\bar{2}\bar{1}\bar{2}]_R$	$[1\bar{1}0\bar{5}]^*_H/[\bar{4}\bar{7}\bar{4}]^*_R$	7.3
$[\bar{1}10\bar{4}]_H/[\bar{5}\bar{2}\bar{5}]_R$	$[1\bar{1}0\bar{4}]^*_H/[\bar{1}\bar{2}\bar{1}]^*_R$	9.1
$[\bar{2}20\bar{5}]_H/[\bar{7}\bar{1}\bar{7}]_R$	$[2\bar{2}0\bar{5}]^*_H/[\bar{1}\bar{3}\bar{1}]^*_R$	14.4
$[\bar{1}10\bar{2}]_H/[\bar{1}0\bar{1}]_R$	$[1\bar{1}0\bar{2}]^*_H/[\bar{1}\bar{4}\bar{1}]^*_R$	17.8
$[\bar{4}40\bar{5}]_H/[\bar{3}\bar{1}\bar{3}]_R$	$[\bar{4}40\bar{5}]^*_H/[\bar{1}(\bar{1}\bar{3})\bar{1}]^*_R$	27.2
$[\bar{1}10\bar{1}]_H/[\bar{2}\bar{1}\bar{2}]_R$	$[1\bar{1}0\bar{1}]^*_H/[0\bar{1}0]^*_R$	32.7

alternation of planes $(\bar{1}\bar{1}20)$, in the plane of which the main rotation took place. This result is consistent with the simulated images in Fig. 3, *d* and *e* constructed according to the condition (3). A similar procedure was performed for the axes of the zone $[\bar{1}101]$ matrix and $[1\bar{1}0\bar{1}]^*$ inclusions for which differences in the diffraction pattern they are more explicit in nature. In addition, the goniometer rotation angles were monitored when moving from one zone axis to another. The values obtained correspond to the difference between the angles (table).

4. Conclusion

The above approach to the identification of inclusions of 60°-rotation domains in films of the metastable phase α-Ga_2O_3 on substrates α-Al_2O_3 consists in the correct choice of the zone axis of the reflecting planes, obtaining and analyzing HRTEM- and STEM-images. To evaluate the type of inclusions, it is necessary to prepare oriented samples. To detect inclusions in the cross section, the sample should be oriented along the axes of the zone type $\langle 11\bar{2}0\rangle$. Samples of planar geometry should be tilted. Then inclusions will appear against the background of the matrix in the scanning mode due to the difference in diffraction conditions during the passing of differently oriented crystal structures. To identify their type, it is necessary to bring into reflection the planes belonging to such a zone axis, which provides a difference in the patterns of electronic microdifraction, and to compare them with model images.

It is established that inclusions of 60°-rotation domains arise at the interface with the substrate and extend to the surface of the layer. Their transverse dimensions reach several tens of nanometers. The fraction of the area in the sample cross-section occupied by inclusions of rotation domains is $\sim 5\%$. Provided that inclusions have flat vertical boundaries, the estimate of their volume fraction does not exceed 5%.

Funding

The work was carried out with the support of the RFBR. Grant No. 19-29-12041mk.

Conflict of interest

The authors declare that they have no conflict of interest.

References

[1] E. Ahmadi, Y. Oshima. J. Appl. Phys. **126**, 160901 (2019). doi: 10.1063/1.5123213
[2] T. Onuma, S. Saito, K. Sasaki, T. Masui, T. Yamaguchi, T. Honda, M. Higashiwaki. Jpn. J. Appl. Phys. **54**, *11*, 112601 (2015). doi: 10.7567/JJAP.54.112601
[3] S.J. Pearton, J. Yang, P.H. Cary, F. Ren, J. Kim, M.J. Tadjer, M.A. Mastro. Appl. Phys. Rev. **5**, 1 (2018). doi: 10.1063/1.5006941
[4] J.P. Remeika, M. Marezio. Appl. Phys. Lett. **8**, *4*, 87 (1966). doi: 10.1063/1.1754500
[5] Y. Oshima, K. Kawara, T. Shinohe, T. Hitora, M. Kasu, S. Fujita. APL Mater. **7**, 2 (2019). doi: 10.1063/1.5051058
[6] A.I. Pechnikov, S.I. Stepanov, A.V. Chikiryaka, M.P. Scheglov, M.A. Odnobludov, V.I. Nikolaev. Semiconductors **53**, *6*, 780 (2019). doi: 10.1134/S1063782619060150
[7] M. Oda, T. Tokuda, H. Kambara, T. Tanikawa, T. Sasaki, T. Hitora. Appl. Phys. Express 9, 021101 (2016). doi: 10.7567/APEX.9.021101
[8] M. Marezuo, J.P. Remeika. J. Chem. Phys. **46**, *5*, 1862 (1967). doi: 10.1063/1.1840945
[9] K. Kaneko, H. Kawanowa, H. Ito, S. Fujita. Jpn. J. Appl. Phys. **51**, 020201 (2012). doi: 10.1143/JJAP.51.020201
[10] Y. Li, X. Xiu, W. Xu, L. Zhang, H. Zhao, Z. Xie, T. Tao, P. Chen, B. Liu, R. Zhang, Y. Zheng. Superlat. Microstruct. **152**, *4*, 106845 (2021). doi: 10.1016/j.spmi.2021.106845
[11] T. Oshima, T. Okuno, S. Fujita. Jpn. J. Appl. Phys. **46**, *11*, 7217 (2007). doi: 10.1143/JJAP.46.7217
[12] V. Gottschalch, K. Mergenthaler, G. Wagner, J. Bauer, H. Paetzelt, C. Sturm, U. Teschner. Phys. Status Solidi **206**, *2*, 243 (2009). doi: 10.1002/pssa.200824436
[13] H. Nishinaka, H. Komai, D. Tahara, Y. Arata, M. Yoshimoto. Jpn. J. Appl. Phys. **57**, *11*, 1 (2018). doi: 10.7567/JJAP.57.115601
[14] I. Cora, F. Mezzadri, F. Boschi, M. Bosi, M. Čaplovičová, G. Calestani, I. Dódony, B. Pécz, R. Fornari. Cryst. Eng. Commun. **19**, *11*, 1509 (2017). doi: 10.1039/c7ce00123a
[15] I. Cora, Z. Fogarassy, R. Fornari, M. Bosi, A. Rečenik, B. Pécz. Acta Mater. **183**, *1*, 216 (2020). doi: 10.1016/j.actamat.2019.11.019
[16] D. Shinohara, S. Fujita. Jpn. J. Appl. Phys. **47**, *9*, 7311 (2008). doi: 10.1143/JJAP.47.7311
[17] Y. Oshima, E.G. Víllora, K. Shimamura. Appl. Phys. Express **8**, *5*, 4 (2015). doi: 10.7567/APEX.8.055501
[18] International tables for crystallography. V.A. / Ed. Th. Hahn. Dordrecht, Reidel (1983). P. 182−189.